



ELSEVIER

Available online at [www.sciencedirect.com](http://www.sciencedirect.com)

Physica A ■■■■ ■■■■■■

PHYSICA A

[www.elsevier.com/locate/physa](http://www.elsevier.com/locate/physa)

# Phase transitions of the energy-relative enstrophy theory for a coupled barotropic fluid–rotating sphere system

Xueru Ding, Chjan C. Lim\*

*Mathematical Sciences, RPI, Troy, NY 12180, USA*

Received 8 March 2006; received in revised form 6 August 2006

## Abstract

The statistical equilibrium of a coupled barotropic fluid–rotating solid sphere system is simulated using an energy-relative enstrophy spherical model in a wide range of parameter space by Monte Carlo (MC) methods [J.M. Hammersley, D.C. Handscomb, Monte Carlo Methods, Methuen & Co, London, Wiley, New York City, 1964; C.C. Lim, J. Nebus, Vorticity, Statistical Mechanics and Simulations, Springer, Berlin, 2006]. The energy-relative enstrophy model does not have the low temperature defect of the classical energy–enstrophy theory [R.H. Kraichnan, Statistical dynamics of two-dimensional flows, *J. Fluid Mech.* 67 (1975) 155–175] because of its microcanonical constraint on relative enstrophy. This model also differs from previous work in not fixing the angular momentum. A family of spin–lattice *hamiltonians* are derived as convergent finite dimensional approximations to the total kinetic energy. MC simulations are used to calculate the mean nearest neighbor parity as order parameter or indicator of phase transitions in the system.

We find that at extremely high energy levels or small negative temperatures, the preferred state is a super-rotational equilibrium state aligned with the planetary spin. This phenomenon has been observed in the Venusian middle atmosphere for many decades but remains difficult to explain [<http://www-atm.physics.ox.ac.uk/project/virtis/venus-super.html>]. For large values of the planetary spin compared with the relative enstrophy there appears to be two phase transitions when the temperature varies from a numerically large negative value to a large positive value. The latter arises as constrained energy minimizers.

© 2006 Published by Elsevier B.V.

*Keywords:* Coupled barotropic fluid–rotating sphere system; Phase transition; Monte Carlo simulations; Energy-relative enstrophy spherical model; Super-rotation

## 1. Introduction

Consider the coupled system consisting of a rotating high-density rigid sphere of radius  $R$ , enveloped by a thin shell of barotropic (nondivergent) fluid. The barotropic flow is assumed to be inviscid, apart from an ability to exchange angular momentum and energy with the heavy solid sphere. In addition we assume that the fluid is in radiation balance and there is no net energy gain or loss from insolation. This provides a crude

\*Corresponding author.

*E-mail addresses:* [dingx@rpi.edu](mailto:dingx@rpi.edu) (X. Ding), [limc@rpi.edu](mailto:limc@rpi.edu) (C.C. Lim).

1 model of the complex planet–atmosphere interactions, including the enigmatic torque mechanism responsible  
2 for the phenomenon of atmospheric super-rotation.

3 We report in this paper the results of simulating an equilibrium statistical mechanics model where we  
4 consider the sphere to have infinite mass and angular momentum. In this case, the sphere serves as reservoirs  
5 of energy and angular momentum and the active part of the model is just the barotropic fluid. Unlike the  
6 barotropic vorticity equation (BVE) that describes the evolution of a homogeneous, nondivergent and  
7 incompressible barotropic flow on the surface of the sphere, our model does not conserve energy nor angular  
8 momentum of the fluid. Recognizing for the moment that some constraint on the relative enstrophy will be  
9 needed to formulate a well-defined model, another point where the current model differs from the classical  
10 energy–enstrophy models is the important one of a microcanonical enstrophy constraint rather than a  
11 canonical constraint. The detailed arguments that was used to formulate this particular version of the  
12 spherical model [1–3] can be found in another paper [4].

13 One of the motivations for working with the current model is indeed the fact that previous efforts based on  
14 the classical doubly-canonical formulation of the energy-relative enstrophy theory for the BVE such as Refs.  
15 [5,6] have failed to discover any phase transitions that could possibly be related to super-rotating flows.  
16 Preliminary reports of related results can be found in proceedings of the American Meteorological Society  
17 Atlanta 2006 Meeting [7,8].

## 19 2. Physical quantities of the model

21 For a problem concerning super-rotating flows on a rotating spherical surface there is little doubt that one  
22 of the key variables is angular momentum of the fluid. The total angular momentum of the fluid and solid  
23 sphere is a conserved quantity. But since we treat the solid sphere as having infinite mass in this model, we  
24 need only track the variable angular momentum of the fluid component of the coupled system.

25 It is clear that a quasi-2D geophysical relaxation problem such as this one, will involve energy and  
26 enstrophy. The total energy of the fluid and sphere is conserved in any frame, both rotating and inertial ones.  
27 Again because of our assumption that the solid sphere has infinite mass, it is only necessary to track the kinetic  
28 energy of the barotropic fluid, which has no gravitational potential energy since it has uniform thickness and  
29 density, and its upper surface is a rigid lid.

30 The barotropic kinetic energy of the fluid component measured in the rest frame, is given in terms of an  
31 arbitrary frame rotating at angular velocity  $\Omega$  by

$$33 \quad H[q] = \frac{1}{2} \int_{S^2} dx [(u_r + u_p)^2 + v_r^2] = \frac{1}{2} \int_{S^2} dx [(u_r^2 + v_r^2) + 2u_r u_p] + \frac{1}{2} \int_{S^2} dx u_p^2$$

$$35 \quad = -\frac{1}{2} \int_{S^2} dx \psi q + \frac{1}{2} \int_{S^2} dx u_p^2,$$

37 where  $u_r = u - u_p$  is the relative zonal velocity,  $\psi$  is the stream function for the relative flow and

$$39 \quad q = \omega + 2\Omega \cos \theta = \Delta\psi + 2\Omega \cos \theta$$

41 is the vorticity in the rest frame in terms of the relative vorticity  $\omega$  and the planetary vorticity  $2\Omega \cos \theta$ ; here  $\theta$   
42 denotes co-latitude on the unit sphere  $S^2$ . Clearly, the value of

$$43 \quad H[q] = H_0[q] = \frac{1}{2} \int_{S^2} dx [u^2 + v^2]$$

45 does not depend on the choice of  $\Omega$ , except that, as will be shown next, by choosing  $\Omega > 0$ , we can conveniently  
46 measure the varying amount of angular momentum in the fluid.

47 Dropping the last term which is a constant and rewriting the rest frame kinetic energy of the fluid (in terms  
48 of relative zonal velocity  $u_r$  and meridional  $v = v_r$ )

$$51 \quad H[q] = \frac{1}{2} \int_{S^2} dx (u_r^2 + v_r^2) + \int_{S^2} dx u_r u_p,$$

we observe that the second term is the projection of relative velocity onto the velocity of a spherical shell

1 rotating at angular velocity  $\Omega$ , which is proportional to the varying net angular momentum of the relative  
 2 flow. In other words, after choosing some convenient fixed spin rate  $\Omega > 0$  to index for example, the rotating  
 3 frame in which the solid sphere is at rest, the fluid could gain or loose angular momentum to the sphere and  
 4 this shows up in the time-varying inner product

$$5 \quad M_\Omega = \int_{S^2} dx u_r u_p.$$

6 Because of its varying second term  $M_\Omega$  this energy is not a Hamiltonian. Indeed, unlike the BVE, there is no  
 7 local in time equations of motion for the fluid component of this model. Instead a generalized variational  
 8 principle based on this energy functional determines its symmetries and dynamical properties. By the  
 9 relationship between a quantum field theory and classical statistical mechanics in one more spatial dimension,  
 10 the partition function for this classical spherical model is mapped onto the path-integral of a nonstandard  
 11 quantum Ising chain and gives a new example of Feynman's generalized least action principle for problems  
 12 that have neither a Hamiltonian nor a Lagrangian.

13 An important conserved quantity in this model is the total circulation

$$14 \quad TC = \int_{S^2} w(x) dx = 0,$$

15 which is a consequence of Stokes Theorem on the sphere. Unlike for the BVE, neither relative enstrophy

$$16 \quad \Gamma_r = \int_{S^2} w^2(x) dx,$$

17 nor total enstrophy

$$18 \quad \Gamma_T = \int_{S^2} q^2 dx,$$

19 can be shown to be invariant in the coupled fluid-sphere model. It is easy to show, however, that the energy  
 20 functional of the model is not well defined without the additional requirement of some constraint on the size of  
 21 its argument, the relative vorticity field. The principle of selective decay or minimum enstrophy which implies  
 22 that only the ratio of energy to enstrophy is relevant to the analysis of asymptotic and statistical equilibrium  
 23 states in macroscopic 2D flows justify fixing the relative enstrophy as the additional constraint for the model.  
 24 Clearly, the statistical mechanics of the above energy functional on iso-enstrophy manifolds is equivalent to  
 25 the statement of this principle. Therefore, unlike the BVE, this microcanonical constraint did not arise from  
 26 the invariance of relative enstrophy.

27 This microcanonical constraint modifies the classical energy–enstrophy theories [5] in substantial ways, chief  
 28 amongst them being removal of the Gaussian low-temperature defect.

29 Higher vorticity moments are not considered in this statistical equilibrium model of 2D geophysical flows  
 30 [5]. A detailed variational analysis of this topic is available in Ref. [9].

### 31 3. Lattice approximation

32 Given  $N$  fixed mesh points  $\vec{x}_1, \vec{x}_2, \vec{x}_3, \dots, \vec{x}_N$  on  $S^2$  and the voronoi cells based on this mesh [10], by  
 33 discretizing the vorticity field as a piecewise constant function, we approximate the relative vorticity

$$34 \quad w(x) = \sum_{j=1}^N s_j H_j(x),$$

35 where  $s_j = w(\vec{x}_j)$  and  $H_j(x)$  is the characteristic function for the domain  $D_j$ , that is

$$36 \quad H_j(x) = \begin{cases} 1, & x \in D_j, \\ 0 & \text{otherwise.} \end{cases}$$

37 The domain  $D_j$  is the subset of the entire domain consisting of points which are closer to  $\vec{x}_j$  than to any other

1 mesh site  $\vec{x}_k$  (also known as voronoi cell). The choice of  $\vec{x}_j$  is arbitrary with one constraint, that the areas  $A_j$  of  
 2 each domain  $D_j$  are approximately equal.

3 This discretization allows us to construct a family of energy functionals by evaluating the rest frame  
 4 barotropic kinetic energy of the fluid,

$$5 \quad H_N[q] = -\frac{1}{2} \int_{S^2} \psi_r q = -\frac{1}{2} \int_{S^2} (w + 2\Omega \cos \theta) \Delta^{-1}(w) \\ 6 \\ 7 \quad = -\frac{1}{2} \left[ \int_{S^2} w \Delta^{-1}(w) + 2\Omega \int_{S^2} \cos \theta \Delta^{-1}(w) \right].$$

8 Since

$$9 \quad \Delta^{-1} H_j(x) = \int_{S^2} G(x, x_j) H_j(x) dx = \int_{D_j} G(x, x_j) dx,$$

10 where  $G(x, x_j) = \Delta^{-1}(\delta(x_j - x))$  represents the fundamental solution to the inverse Laplace–Beltrami operator,  
 11 we get

$$12 \quad \Delta^{-1} w(x) = \Delta^{-1} \left( \sum_{j=1}^N s_j H_j(x) \right) = \sum_{j=1}^N s_j \int_{D_j} G(x, x_j) dx.$$

13 The first term of  $H_N[q]$  is

$$14 \quad -\frac{1}{2} \int_{S^2} w \Delta^{-1}(w) = -\frac{1}{2} \int_{S^2} \sum_{i=1}^N s_i H_i(y) \sum_{j=1}^N s_j \int_{D_j} G(x, x_j) dx dy \\ 15 \\ 16 \quad \simeq -\frac{1}{2} \sum_{i=1}^N \sum_{j \neq i}^N s_i s_j A_i A_j G(x_i, x_j) \\ 17 \\ 18 \quad \simeq -\frac{8\pi^2}{N^2} \sum_{i=1}^N \sum_{j \neq i}^N s_i s_j \ln |1 - x_i \cdot x_j|,$$

19 where  $G(x_i, x_j) = \ln |1 - x_i \cdot x_j|$ ,  $A_i = A_j \simeq 4\pi/N$ , and

$$20 \quad H_i(x) H_j(x) = \begin{cases} 1 & \text{if } i = j, \\ 0 & \text{if } i \neq j. \end{cases}$$

21 The second term of  $H_N[q]$  is

$$22 \quad -\Omega \int_{S^2} \cos \theta \Delta^{-1}(w) dx = -\Omega \int_{S^2} \cos \theta dx \int_{S^2} G(x, y) w(y) dy \\ 23 \\ 24 \quad = \frac{2\pi}{N} \Omega \sum_{j=1}^N s_j \cos \theta_j.$$

25 Finally, we get the spin lattice models

$$26 \quad H_N[q] = -\frac{1}{2} \sum_{i=1}^N \sum_{j \neq i}^N J_{ij} s_i s_j - \sum_{j=1}^N F_j s_j,$$

27 where  $J_{ij} = (16\pi^2/N^2) \ln |1 - x_i \cdot x_j|$  and  $F_j = -(2\pi/N)\Omega \cos \theta_j$ . The external field  $F_j$  comes from the fixed  
 28 rotation rate  $\Omega > 0$  of the solid sphere, and represents the coupling between the local relative vorticity and the  
 29 planetary vorticity field. It is proportional to the net relative angular momentum of the fluid, which as  
 30 discussed in an earlier section, is a time-dependent quantity.

31 In the MC simulations discussed here, we fix the discretized total circulation to be zero and keep the relative  
 32 enstrophy fixed. These quantities are discrete approximations to the first and second moments of the relative  
 33 vorticity field.

1 The truncated relative enstrophy is given by

$$3 \quad \Gamma_r = \int_{S^2} w^2(x) dx = \int_{S^2} \left( \sum_{i=1}^N s_i H_i(x) \right)^2 dx = \sum_{i=1}^N s_i^2 A_i = \frac{4\pi}{N} \sum_{i=1}^N s_i^2 = Q_{rel}$$

5 and the truncated total circulation is

$$7 \quad TC = \int_{S^2} w(x) dx = \int_{S^2} \sum_{i=1}^N s_i H_i(x) dx = \sum_{i=1}^N s_i A_i = \frac{4\pi}{N} \sum_{i=1}^N s_i = 0.$$

#### 11 4. Energy-relative enstrophy theory

13 The equilibrium statistical mechanics models, in for instance Ref. [11], for 2D macroscopic flows are based  
 15 on a Gibbs partition function which is canonical in both the energy and the enstrophy. As shown by  
 17 Frederiksen and Sawford in Ref. [5], their doubly-canonical energy–enstrophy theory for barotropic flows on  
 19 a rotating sphere which conserves both relative enstrophy and angular momentum separately, does not  
 21 support phase transitions. In the current energy-relative enstrophy theory, we relax the angular momentum  
 23 constraint and apply the relative enstrophy constraint microcanonically to capture the full physics of the  
 25 problem. We shall show that treating the coupled barotropic fluid–rotating massive sphere system, and  
 27 thereby relaxing the angular momentum constraint used in previous works, has significant physical  
 29 consequences on the results obtained, namely, two phase transitions between disordered vorticity states and  
 organized super-rotating and sub-rotating flow states. The equilibrium statistical mechanics of this theory on a  
 rotating sphere is formulated on the basis of a canonical constraint on the kinetic energy, and a  
 microcanonical constraint on the relative enstrophy, while the total circulation is set to zero. The  
 microcanonical constraint on the relative enstrophy makes this a version of Kac’s spherical model [2]. Exact  
 solutions of this model will be discussed in another paper [4]. At small absolute values of the statistical  
 temperature of macroscopic flows, the free energy in this model is closely approximated by the internal energy,  
 the properties of which is studied in Ref. [12] using a variational approach.

29 The partition function of the energy-relative enstrophy spherical model is

$$31 \quad Z_N = \int \left( \prod_{j=1}^N ds_j \right) \delta \left( NQ_N - 4\pi \sum_{j=1}^N s_j^2 \right) \exp[-\beta H_N],$$

33 where  $H_N$  is spin–lattice Hamiltonian, and the Gibbs canonical–microcanonical probability is

$$35 \quad P_G = \frac{1}{Z_N} \exp[-\beta H_N] \delta \left( NQ_N - 4\pi \sum_{j=1}^N s_j^2 \right).$$

#### 39 5. Monte Carlo simulations of energy-relative enstrophy model

41 In this paper a MC method based on the Markov Chain algorithm of Metropolis and Hastings [3,13] is  
 43 employed to find several statistical equilibria of the energy-relative enstrophy spherical model. Initially the  
 45 Metropolis–Hastings algorithm is used to generate a mesh of points on the surface of the sphere which covers  
 47 the domain in a reasonably uniform manner [10]. Once this mesh is set, a new round of MC is applied. Initially  
 49 randomly chosen vorticities are given to each mesh site so that the spherical constraints are set. Then during  
 51 this second round the vortices are given strengths which are allowed to vary, provided the circulation and  
 relative enstrophy are held constant. MC simulations in our energy-relative enstrophy model on a rotating  
 sphere conserve both the discrete circulation and the relative enstrophy, and seek statistical equilibria of the  
 lattice system for a wide range of values of inverse temperature  $\beta$ , spin rate  $\Omega$  and relative enstrophy  $Q_{rel}$ . In  
 the following subsections, we will describe diagnostic tools used to extract evidence of phase transitions from  
 the MC simulation data. We will also organize the data into most probable relative vorticity states and by  
 applying a Fourier decomposition procedure-based on the spherical harmonics—to these states, we shall

provide evidence that these states are indeed super-rotating and sub-rotating flow states that contain more and less angular momentum, respectively, than the same fluid shell rotating at the spin rate of the solid sphere.

### 5.1. Super-rotation

When inverse temperature  $\beta$  is negative, the first term of the spin-lattice Hamiltonian

$$H_N[q] = -\frac{8\pi^2}{N^2} \sum_{i=1}^N \sum_{j=1}^N s_i s_j \log |1 - x_i \cdot x_j| + \frac{2\pi}{N} \Omega \sum_{j=1}^N \cos \theta_j s_j,$$

suggests that any vortex surrounded by vortices of the same sign will achieve higher energy; the second term suggests that the sites near the north pole should have the most positive values and those near the south pole should have the most negative values in order to obtain higher energy, since  $\cos \theta$  varies from 1 at north pole to  $-1$  at the south pole.

We find that the most probable vorticity distributions produced by MC simulations of the spherical model at large negative values of  $\beta$  have the form (Fig. 1) suggested by the above heuristic argument. This is a high-energy state (Fig. 1c) and the form of these macrostates is also close to that of the unique global energy maximizer in a variational theory [12]. The color convention in the figure for positive vorticity is red and for negative is blue. The predominance of red colors in the north hemisphere denotes the most probable state for negative  $\beta$  is a super-rotating solid-body flow state.

We show that the components  $\alpha_{lm}$  of the most probable simulated vorticity field  $\omega(x)$  in terms of the orthonormal spherical harmonics  $\psi_{lm}$  in Fig. 1b. Since the spherical harmonics  $\psi_{lm}$  form an orthonormal basis for the associated Hilbert space of square-integrable functions on the surface of the unit sphere,  $\alpha_{lm}$  can be calculated by the inner product of  $\omega(x)$  and  $\psi_{lm}(x)$ , that is  $\alpha_{lm} = \langle \omega(x), \psi_{lm}(x) \rangle = 4\pi/N \sum_{j=1}^N \omega(x_j) \psi_{lm}(x_j)$ .

It is clear that for the super-rotating flow state,  $\psi_{10}$  is the spherical harmonic with the largest amplitude,  $\sqrt{Q_{rel}}$ .

### 5.2. Sub-rotation

When inverse temperature  $\beta$  is large and positive and the relative enstrophy  $Q_{rel}$  is less than  $\Omega^2 C^2$ , we repeatedly find a most probable relative vorticity distribution shown in the Fig. 2 below. In particular, by choosing  $\beta = 2, \Omega = 60$  and  $Q_{rel} = 128$  such that  $Q_{rel} < \Omega^2 C^2$ , we produced the statistical equilibrium state in the figure. This macrostate is largely a counter-rotating flow associated with a nonlinearly stable state achieving local minimum energy (Fig. 2c) with  $w_{\min}^0(Q_{rel}) = -\sqrt{Q_{rel}} \psi_{10}$  in the variational theory [12].

The predominance of blue colors in the northern hemisphere and red colors in the southern hemisphere denotes the most probable state is a sub-rotation state (Fig. 2a). Also Fig. 2b gives the largest component of the sub-rotating relative vorticity is again the harmonic  $\psi_{10}$  with a negative amplitude.

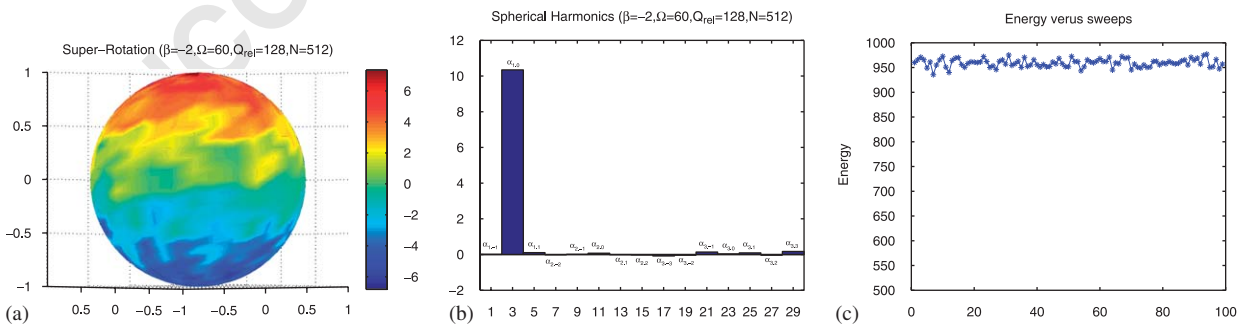


Fig. 1. Positive  $\beta$ —super-rotation. In this example there are 512 points,  $\beta = -2$  and run for 10,000 sweeps.



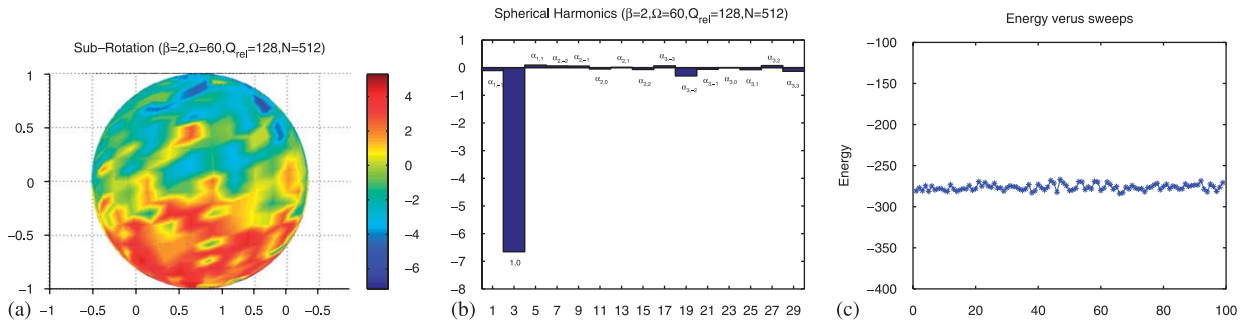


Fig. 2. Positive  $\beta$ —sub-rotation. In this example there are 512 points,  $\beta = 2$  and run for 10,000 sweeps.

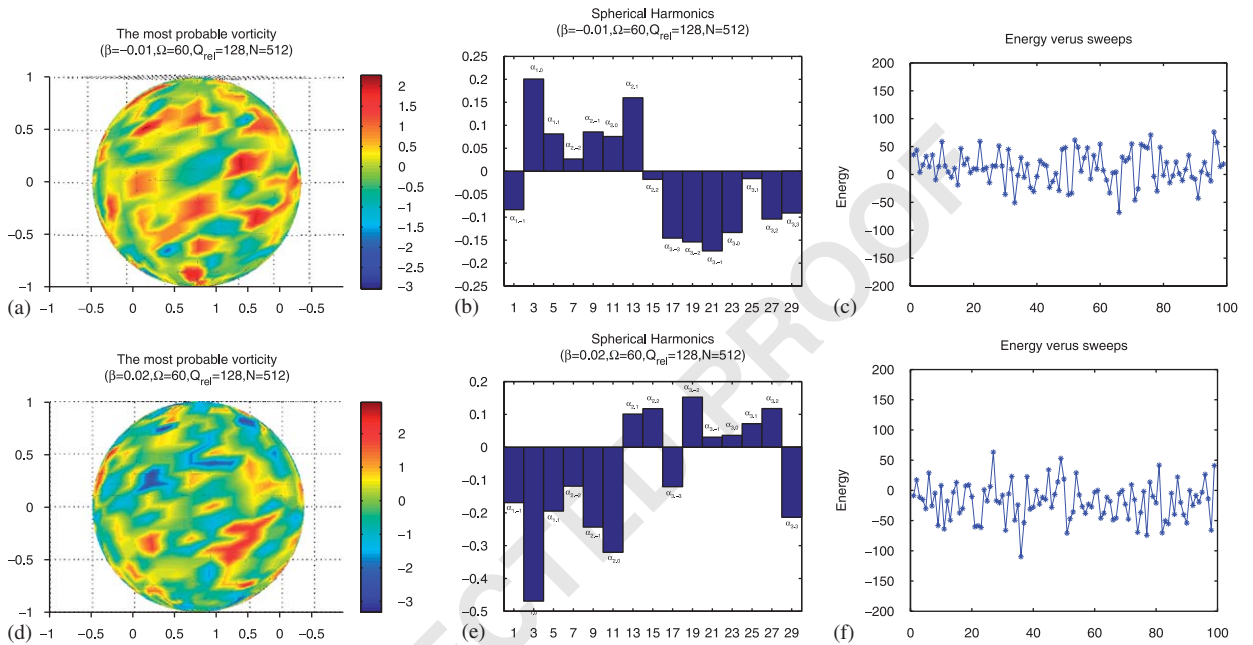


Fig. 3. The most probable state with  $\beta = -0.01$  and  $0.02$ ,  $N = 512$  and run for 10,000 sweeps.

### 5.3. Phase transitions

Extensive simulations of this model over a wide range of parameters, namely inverse temperature, spin rate of solid sphere and relative enstrophy indicate that there are two phase transitions, at a negative critical temperature for all values of spin and at a positive critical temperature when the planetary spin is large enough compared to the relative enstrophy.

In particular, by choosing spin rate  $\Omega = 60$ , relative enstrophy  $Q_{rel} = 128$  and the number of the lattice  $N = 512$  as we did for super- and sub-rotation, we found evidence for those phase transitions. There are two equilibrium states with  $\beta = -0.01$  and  $0.02$  shown in Fig. 3. The energies in those cases never settle, and they fluctuate wildly while the simulation runs (Fig. 3c and f). A comparison of those two pictures with the Figs. 1 and 2, suggests that there are phase transitions between  $\beta = -0.01$  to  $-2$  and  $0.02$  to  $-2$ .

In order to extract more substantial evidence of phase transitions [1] from the data, we will now describe a useful diagnostic tool which is related to those used to measure correlations in MC data.

### 1 5.3.1. Mean nearest neighbor parity

We should be able to determine whether a system is in the organized or mixed state given the site strengths and mesh positions. To estimate what state systems are in, we introduce the mean nearest neighbor parity as a diagnostic tool for determining properties of the order parameter and to measure correlations [10]. Let us define the parity of a pair of sites to be the product of the signs of one site of the pair's vorticity with the sign of the vorticity of the other site. That means when the pair have same signs it will be 1; when the pair has opposite signs it is  $-1$ ; and in case either site is 0 it is 0. For site  $j$ , the nearest neighbor  $k$  is the site closest to it. The nearest neighbor parity is then the parity of the pair of points  $j$  and  $k$ . Let the mean nearest neighbor parity be the arithmetic mean of the nearest neighbor parities for each nearest neighbor pair. This property provides an excellent measure for the structure of site vorticities. When sites are generally organized the mean nearest neighbor parity is close to 1, and for mixed state the mean nearest neighbor parity is close to 0.

Since by the mean nearest neighbor parity we can find whether the system is in an unmixed state or a mixed state, we can search for the evidence suggesting the phase transitions as the temperature changes.

15

17

19

21

23

25

27

29

31

33

35

37

39

41

43

45

47

49

51

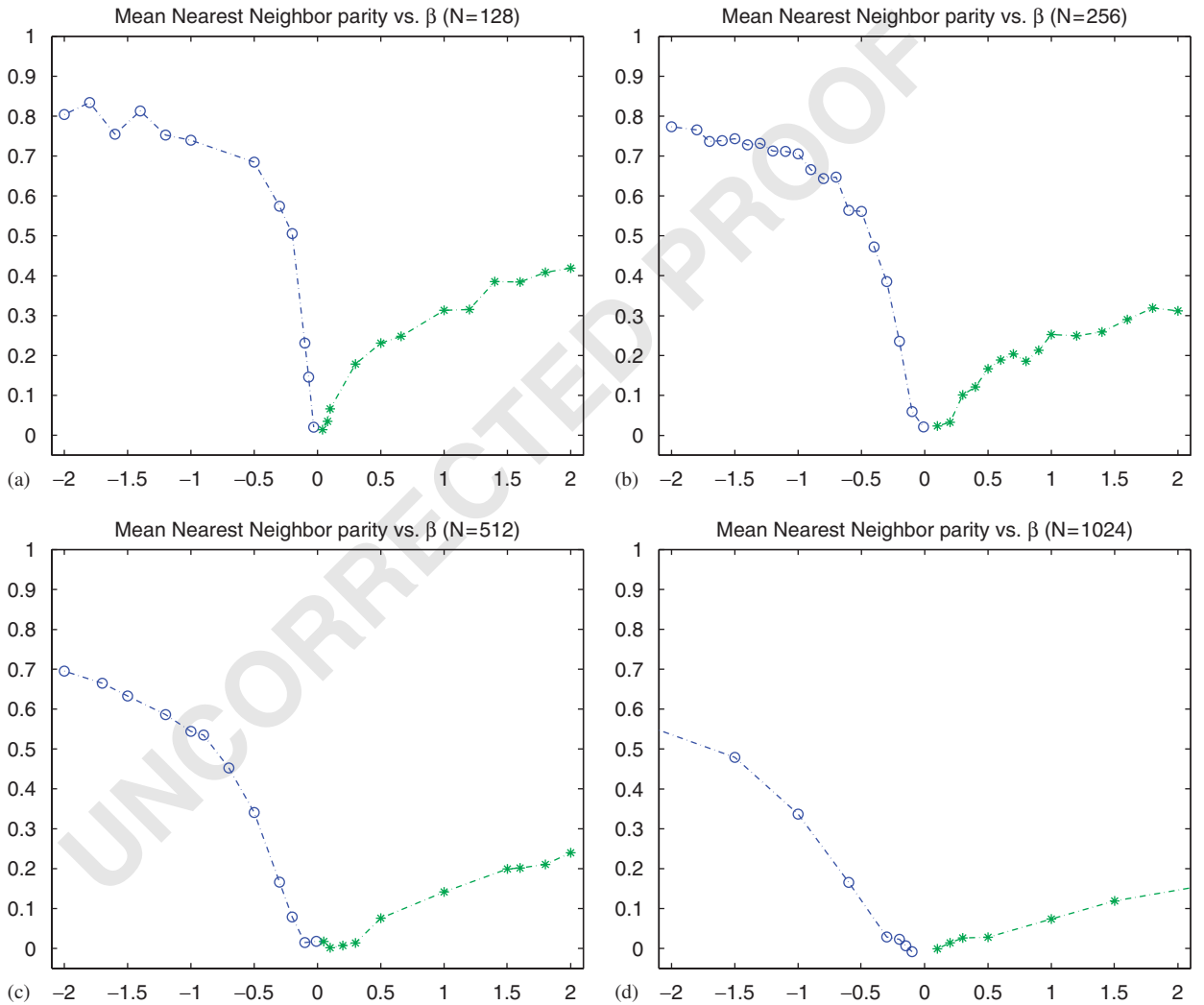


Fig. 4. The mean nearest parity with different  $N$  vs. inverse temperatures on a range from  $\beta = -2$  to 2 with fix the relative enstrophy  $Q_{rel} = 128$  and spin rate  $\Omega = 60$ .



1 Our first experiment fixes the relative enstrophy  $Q_{rel}$  and spin rate  $\Omega$ , then allows the mesh size  $N$  to vary.  
 2 The parity drops to zero in both negative and positive inverse temperature  $\beta$  in Fig. 4, suggesting there may be  
 3 two phase transitions in both the negative and positive temperature regions on the rotating sphere.

4 Let us consider the regions of negative and positive  $\beta$  where the mean nearest neighbor parity drops from a  
 5 large number to zero. We choose the curves of data points to fit the typical curve we see in the two phase  
 6 transitions, let  $m(\beta) = C^\pm(1 - (\beta_c^\pm/\beta)^\alpha)$  for some scaling constants  $C^\pm$  (see Table 1). In all those cases we find  
 7  $\alpha = 1$  can always fit well (Fig. 5). This property strongly suggests that the mean field theory is exact for this  
 8 type of problem [1,14].  
 9

### 5.3.2. Specific heat

10 Evidence for the phase transitions also can be found in the specific heat measurements. Specific heat may be  
 11 calculated by numerical differentiation of the internal energy with respect to the temperature,  
 12

$$13 \quad C_v \left( \frac{k_B T_{n+1} + k_B T_n}{2} \right) = \frac{U(k_B T_{n+1}) - U(k_B T_n)}{k_B T_{n+1} - k_B T_n},$$

14 where  $U(k_B T_n)$  is the internal energy at the temperature  $k_B T_n$ , and  $k_B$  is Boltzmann's constant.  
 15  
 16  
 17

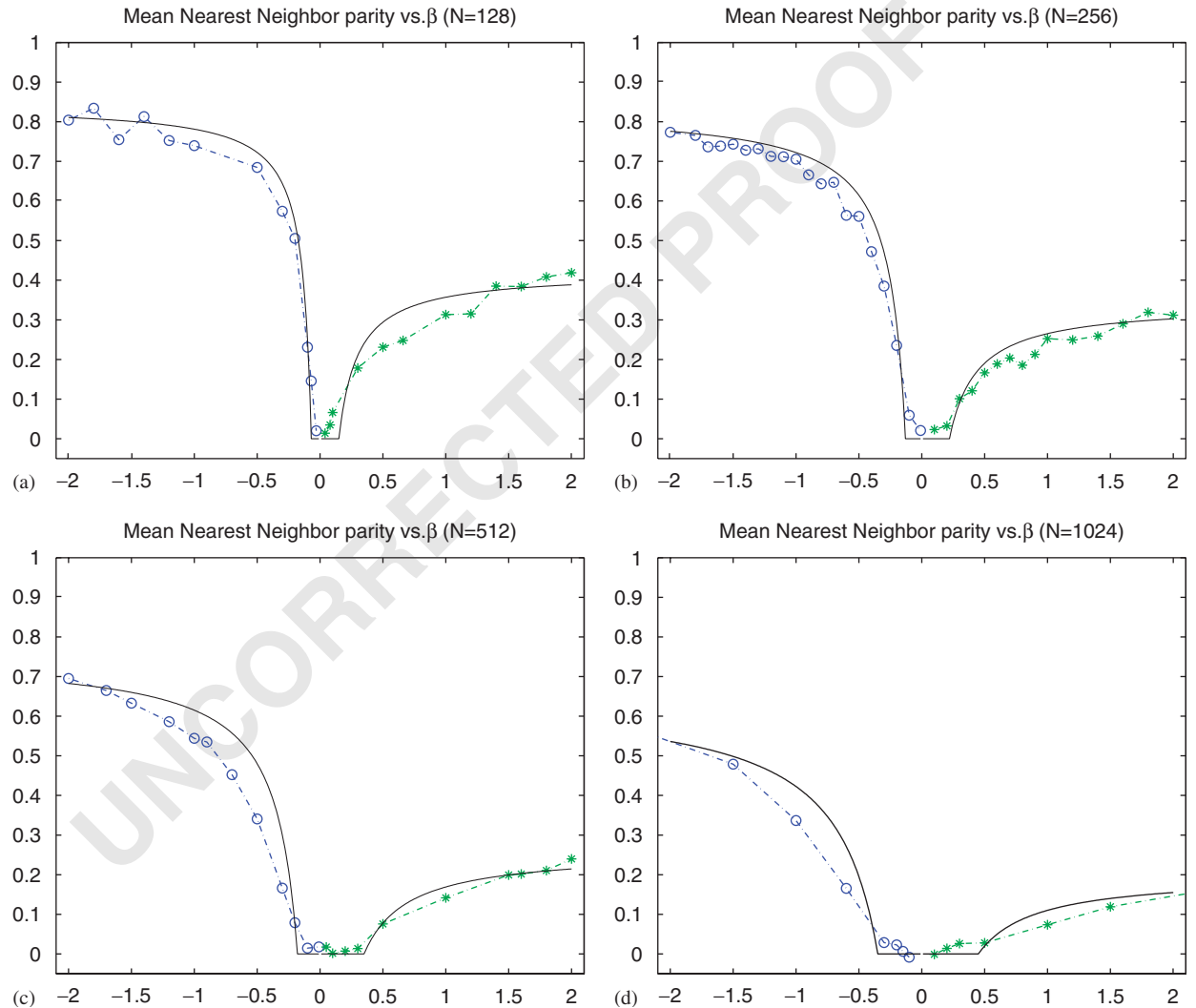
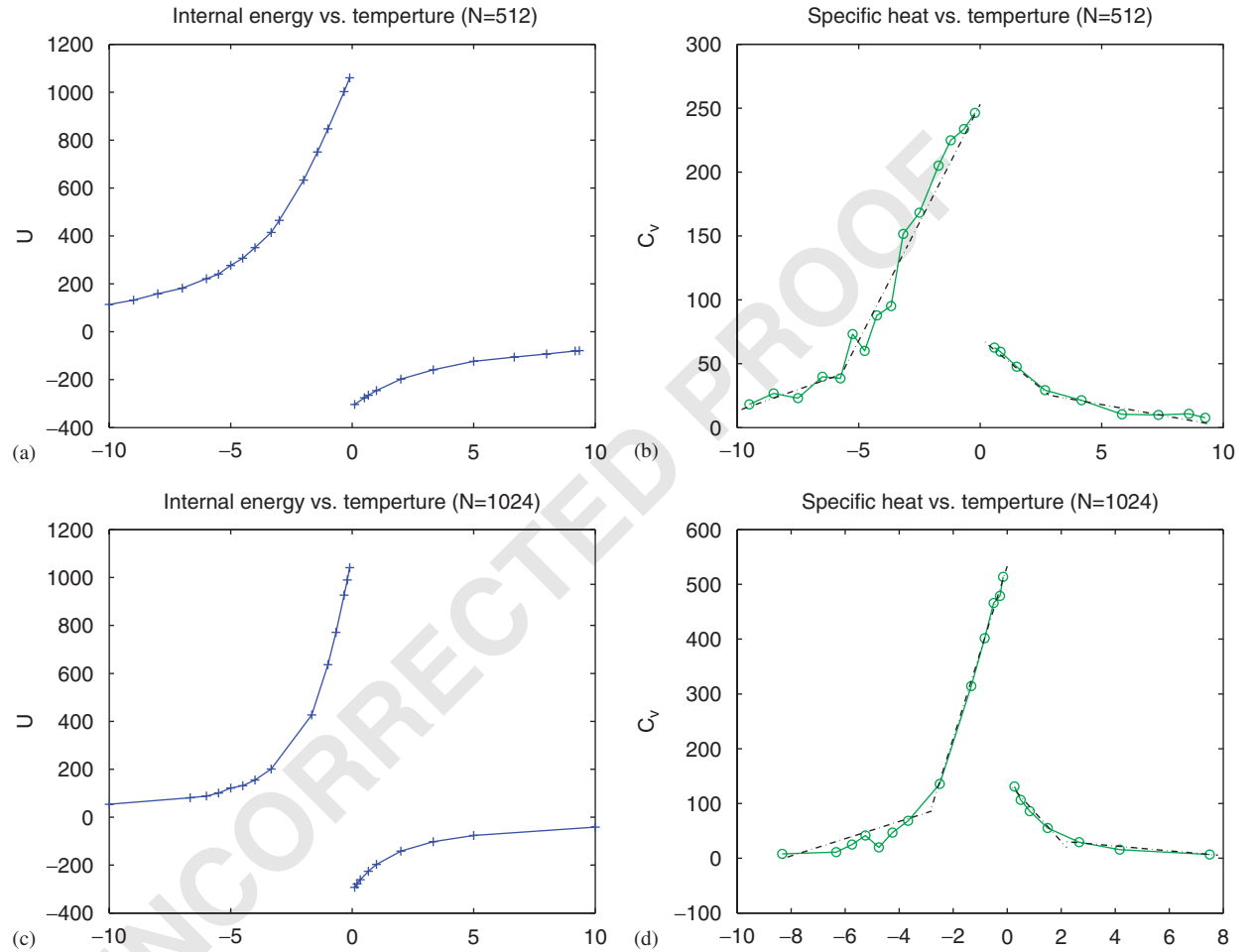


Fig. 5. The mean nearest neighbor parity and fitting curves with different  $N$ .

Table 1

$N$	128	256	512	1024
$C^+$	0.42	0.34	0.26	0.20
$C^-$	0.84	0.82	0.75	0.60
$\beta_c^+$	0.15	0.22	0.35	0.45
$\beta_c^-$	0.0012	0.00086	0.00068	0.00044
$\frac{N}{\beta_c^-}$	-0.07	-0.13	-0.18	-0.35
$\frac{\beta_c^-}{N}$	-0.00055	-0.00051	-0.00035	-0.00034

Fig. 6. The internal energy  $U$  and specific heat  $C_v$  vs. temperature  $k_B T$ .

In Fig. 6, we show the internal energy and specific heat as functions of temperature for the cases of  $N = 512$  and 1024. As the dashed lines shown in Fig. 6b and d, there are discontinuities in the first derivative of specific heat with respect to temperature, which correspond to two phase transitions at both positive and negative temperatures. These results (see Table 2) agree very well with the inverse critical temperatures  $\beta_c^\pm$  we found in Table 1, here  $\beta_c^\pm$  is equal to  $1/k_B T_c^\pm$ .

1 Table 2

3	$N$	512	1024
5	$k_B T_c^+$	2.8	2.2
5	$k_B T_c^-$	-5.7	-2.8

7

9

11

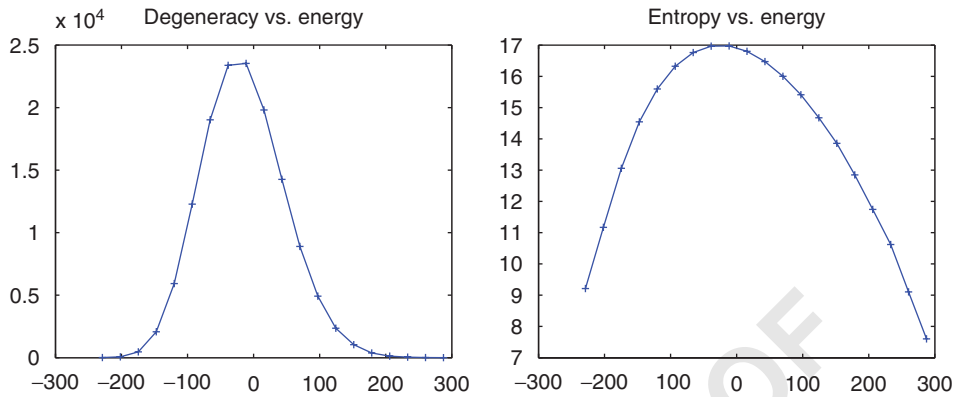
13

15

17

19

21



23 Fig. 7. Degeneracy and entropy vs. energy.

25 The temperature in our system is the macroscopic flow temperature, so it does not correspond to the  
 27 ~~measuring heat or~~ molecular motions. In Statistical mechanics the temperature is defined as the derivative of  
 entropy with respect to the entropy. Although there is no physical heat in our problem, it still has temperature.

## 29 6. Free energy

31 The MC method is an algorithm capable of the numerical estimation of any quantity which can be written  
 33 as the average of a state function. The estimation of the entropy, however, is a difficult task since there is no  
 state function whose average is the entropy. The same can be said about the free energy. To overcome this  
 difficulty we introduce a new method to estimate the entropy of the spin lattice system by MC simulation.

35 This approach is based on the probability distribution of states, in which the probability of occurrence of a  
 37 configuration with energy  $E$  is proportional to  $\exp(-\beta E)$ . Following the usual Metropolis MC procedure, the  
 probability of moving from state  $A$  to  $B$  is defined as  $\exp(-\beta(E_B - E_A))$ . We notice when we set  $\beta = 0$  the  
 39 probability from state  $A$  to  $B$  should be 1 all the time no matter if  $(E_B - E_A)$  is positive or negative. That  
 means the new states would always be accepted. Hence, this new method simulates the system with the same  
 41 probability for all the states, and after enough sweeps this special MC simulation (with  $\beta = 0$ ) should  
 randomly walk though all parts of system's energy space.

43 We will enumerate the different states of the system by their energy, dividing the energy into 20 levels from  
 the low to high in values. The entropy  $S(E)$  is proportional to the logarithm of degeneracy—the number of  
 45 configuration in the corresponding macrostates by Boltzmann's entropy equation  $S(E) = k_B \ln W$ , where  $W$  is  
 the degeneracy of a given macrostate.

47 Fig. 7 shows that the degeneracy and entropy ( $k_B = 1$ ) decline as the energy approaches the maximum,  
 thereby confirming the phenomenon of negative temperature—the derivative of entropy with respect to energy  
 is negative.

49 We use Gibbs's free energy formula  $F = U - TS$  and our entropy calculation method to get the free energy  
 in Fig. 8. MC simulations predict a super-rotating most probable state with extremely high energy and low  
 51 entropy, and a sub-rotating most probable flow state with very low energy and low entropy when the relative  
 enstrophy is small in comparison to the planetary spin. This suggests that the maximal kinetic energy steady-

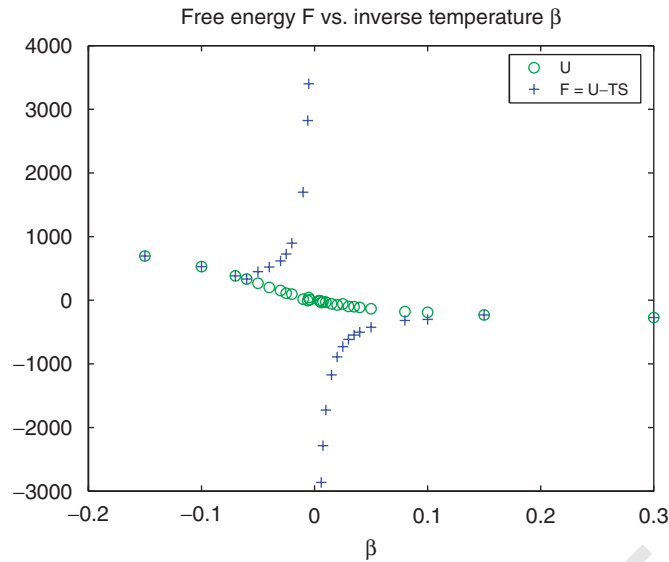


Fig. 8. Free energy  $F$  and internal energy  $U$  vs. inverse temperature.

state from two zero temperature variational theory [12] should be related to the most probable flow state predicted by MC simulation at hot enough negative temperatures; similarly, the minimal kinetic energy steady-state from that theory is related to the most probable flow state at low positive temperatures. At temperatures with sufficiently small absolute values, and provided that the entropy–energy relationship in this problem is as depicted in the above figure, this correspondence between the variational theory and the statistical equilibrium theory follows directly from the form of the Gibbs’s free energy  $F = U - TS \simeq U$ .

## 7. Conclusion

In summary, we have shown that the energy-relative entrophy model supports the super- and sub-rotation flow states, provided the spin rate is positive. The main simulation result in the case of nonzero spin rate finds evidence of a phase transition at negative temperatures and another at positive temperatures. The phase transition occurs between disordered states with zero net angular momentum which hold at inverse temperatures less than  $|\beta_c^\pm|$ , and the distinguished ordered state at all inverse temperatures greater than  $|\beta_c^\pm|$ . The results reported here suggest that a correct statistical mechanics theory for the coupled barotropic fluid–rotating sphere system—one where the fluid can exchange angular momentum with the massive rotating sphere—can provide qualitative explanations and predictions of the enigmatic super-rotation and sub-rotation phenomena in planetary atmosphere [15].

## 8. Uncited reference

[18]. remove ref [18] from paper and remove section 8. Uncited reference

## Acknowledgments

This work is supported by ARO Grant W911NF-05-1-0001 and DOE Grant DE-FG02-04ER25616. We would like to thank Dr. Joseph Nebus for help with initial development of our Monte Carlo simulation code. We independently discovered the method for computing the entropy, but found the Refs. [16,17] in which the authors talked about similar ideas to get entropy and free energy after this paper was accepted.

1 **References**

- 3 [1] H.E. Stanley, Introduction to Phase Transitions and Critical Phenomena, Oxford University Press, New York, 1971.  
 4 [2] T.H. Berlin, M. Kac, The spherical model of a ferromagnet, *Phys. Rev.* 86 (1952) 821–835.  
 5 [3] C.C. Lim, J. Nebus, Vorticity, *Statistical Mechanics and Simulations*, Springer, Berlin, 2006.  
 6 [4] C.C. Lim, A spherical model for coupled barotropic fluid–rotating sphere system and condensation of energy into super-rotation  
 7 ground states, Preprint, 2006.  
 8 [5] J.S. Frederiksen, B.L. Sawford, Statistical dynamics of 2D inviscid flow on a sphere, *J. Atmos. Sci.* 37 (1980) 717–732.  
 9 [6] J.S. Frederiksen, Eastward and westward flows over topography in nonlinear and linear barotropic models, *J. Atmos. Sci.* 39 (1982)  
 10 2477–2489.  
 11 [7] X. Ding, C.C. Lim, Equilibrium phases in a energy-relative enstrophy statistical mechanics model of barotropic flows on a rotating  
 12 sphere—non-conservation of angular momentum, *American Meteorological Society Proceedings*, Atlanta, 2006.  
 13 [8] R.S. Mavi, C.C. Lim, Phase transitions of barotropic flows on a rotating sphere—non-conservation of angular momentum, *American  
 14 Meteorological Society Proceedings*, Atlanta, 2006.  
 15 [9] C.C. Lim, J. Shi, The role of higher vorticity moments in a variational formulation of barotropic flows on a rotating sphere, Preprint,  
 16 2005.  
 17 [10] C.C. Lim, J. Nebus, The spherical model of logarithmic potentials as examined by Monte Carlo methods, *Phys. Fluids* 16 (10) (2004)  
 18 4020–4027.  
 19 [11] R.H. Kraichnan, Statistical dynamics of two-dimensional flows, *J. Fluid Mech.* 67 (1975) 155–175.  
 20 [12] C.C. Lim, Energy extremals and nonlinear stability in an energy-relative enstrophy theory of a coupled barotropic fluid–rotating  
 21 sphere system, *J. Math. Phys.* (2006), accepted for publication.  
 22 [13] J.M. Hammersley, D.C. Handscomb, *Monte Carlo Methods*, Methuen & Co, London, Wiley, New York City, 1964.  
 23 [14] G. Morandi, F. Napoli, E. Ercolessi, *Statistical Mechanics: An Intermediate Course*, World Scientific, Singapore, 2001.  
 [15] (<http://www-atm.physics.ox.ac.uk/project/virtis/venus-super.html>).  
 [16] B.A. Berg, Multicanonical recursions, *J. Stat. Phys.* 82 (1996) 323.  
 [17] M.J. Thill, On the free energy Monte Carlo algorithm, cond-mat/9703234, 1997.  
 [18] C.C. Lim, Exact solution of an energy-enstrophy theory for the barotropic vorticity equation on a rotating sphere, *Physica A* 290  
 (2001) 131–158.  
 delete ref [18] from paper  
 ref [12] *J. Math. Phys.* (2007), in press, June 2007.